Acta Pharmaceutica Sinica B 2019;9(1):107–117

Chinese Pharmaceutical Association
Institute of Materia Medica, Chinese Academy of Medical Sciences

Acta Pharmaceutica Sinica B

www.elsevier.com/locate/apsb
www.sciencedirect.com

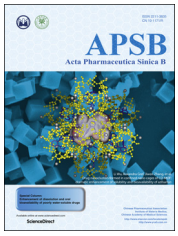

ORIGINAL ARTICLE

Supersaturated polymeric micelles for oral silybin delivery: the role of the Soluplus–PVPVA complex ☆

Chunliu Zhu[a,c], Shuang Gong[b,c], Jinsong Ding[b], Miaorong Yu[c], Ejaj Ahmad[c], Yi Feng[a,*], Yong Gan[c,*]

[a]*Engineering Research Center of Modern Preparation Technology of Traditional Chinese Medicine, Shanghai University of Traditional Chinese Medicine, Shanghai 201203, China*
[b]*Xiangya School of Pharmaceutical Science, Central South University, Changsha 410000, China*
[c]*Shanghai Institute of Materia Medica, Chinese Academy of Science, Shanghai 201203, China*

Received 13 April 2018; received in revised form 12 July 2018; accepted 30 July 2018

KEY WORDS

Silybin;
Soluplus;
PVPVA;
Complex;
Supersaturated drug delivery system;
Oral bioavailability

Abstract Increasing the degree of supersaturation of drugs and maintaining their proper stability are very important in improving the oral bioavailability of poorly soluble drugs by a supersaturated drug delivery system (SDDS). In this study, we reported a complex system of Soluplus–Copovidone (Soluplus–PVPVA) loaded with the model drug silybin (SLB) that could not only maintain the stability of a supersaturated solution but also effectively promote oral absorption. The antiprecipitation effect of the polymers on SLB was observed using the solvent-shift method. In addition, the effects of the polymers on absorption were detected by cellular uptake and transport experiments. The mechanisms by which the Soluplus–PVPVA complex promotes oral absorption were explored by dynamic light scattering, transmission electron microscopy, fluorescence spectra and isothermal titration calorimetry analyses. Furthermore, a pharmacokinetic study in rats was used to demonstrate the advantages of the Soluplus–PVPVA complex. The results showed that Soluplus and PVPVA spontaneously formed complexes in aqueous solution *via* the adsorption of PVPVA on the hydrophilic-hydrophobic interface of the Soluplus micelle, and the Soluplus–PVPVA complex significantly increased the absorption of SLB. In conclusion, the Soluplus–PVPVA complex is a potential SDDS for improving the bioavailability of hydrophobic drugs.

*Corresponding authors.
E-mail addresses: fengyi@vip.sina.com (Yi Feng), ygan@mail.shcnc.ac.cn (Yong Gan).

☆Invited for Special Column.

Peer review under responsibility of Institute of Materia Medica, Chinese Academy of Medical Sciences and Chinese Pharmaceutical Association.

https://doi.org/10.1016/j.apsb.2018.09.004

1. Introduction

Supersaturated drug delivery systems (SDDS) are defined as the systems that contain drug molecules in a thermodynamically unstable form or otherwise rapidly dissolving form such that a supersaturated drug solution is generated in the gastrointestinal fluids and maintained for a period of time to promote drug absorption[1,2]. SDDS is different from conventional solubilizing approaches. Its mechanism of promoting absorption is to generate a supersaturated state of the drug and maintain its proper stability, while a solubilized formulation avoids supersaturation by increasing the equilibrium solubility of the drugs[3]. Increasing the equilibrium solubility of the drug often requires a large quantity of solubilization additives such as surfactants. In contrast, only a small quantity of precipitation inhibitor is required for SDDS to maintain a supersaturated state[4]. Therefore, SDDS is applicable to poorly soluble drugs and avoids the digestive toxicity caused by large amounts of surfactants. However, supersaturated solutions are thermodynamically unstable systems, and the high-energy solute molecules have the tendency to recrystallize[5,6]. Thus, how to increase the concentration of the drug and maintain its stability has become the key issue in exploiting SDDSs[7].

Soluplus, a polyvinyl caprolactam-polyvinyl acetate-polyethylene glycol graft copolymer, is a novel amphiphilic polymeric solubilizer that has been widely studied in recent years[8,9]. Due to the presence of both hydrophilic and hydrophobic chains within Soluplus molecules, they can form micelles even at a very low concentration in aqueous solution, and as a consequence, the solubility of poorly water-soluble drugs can be greatly enhanced[10–12]. The presence of hydrophobic chains in Soluplus makes it an effective inhibitor to prevent precipitation and a good candidate for supersaturated preparations[13–15]. However, our group found that the interactions between the active ingredient and Soluplus caused drug retention in the hydrophobic core of the micelle, which is not conducive to the absorption of the encapsulated drug[16]. Since the main absorption mechanism of a supersaturated solution is the passive diffusion of the free drug, the presence of solubilizing excipients such as polymers, surfactants, or cyclodextrins would hamper the transmembrane transport[17]. The flux is directly proportional to the solute activity, while the presence of solubilizer reduces the activity of dissolved molecules, leading to reduce flux. The change in the relationship between flux and solute concentration in the presence of solubilizing excipients can be seen in the pharmaceutical literature[17–19]. Only unionized free drugs can be effectively absorbed by passive diffusion[20]. Therefore, we envisioned weakening the interaction between Soluplus and the drug to increase the concentration of free drug without compromising the antiprecipitation ability. The antiprecipitation ability of polymers is related to the interactions between the polymer and drug, and modulating the hydrophobic core of the polymeric micelles can effectively change the drug release behavior[21,22]. PVPVA, *N*-vinylpyrrolidone and vinyl acetate water soluble copolymer has been reported to form complexes with sodium lauryl sulfate (SLS), and the formation of these complexes decreased the intensity of the interactions between PVPVA and the drug[23]. Therefore, we speculate that the amphiphilic Soluplus, like SLS, can form complexes with PVPVA to achieve the desired stable state of the supersaturated drug solution.

In this work, we used the poorly insoluble drug silybin (SLB) as the model drug, and Soluplus and PVPVA as the vehicle to design a supersaturated polymeric micelle system. The effects of polymers on absorption were detected by cellular uptake and transport experiments. In addition, the mechanisms by which the Soluplus–PVPVA complex promotes oral absorption were explored. A pharmacokinetic study in rats was also used to demonstrate the advantages of the Soluplus–PVPVA complex. This system could maintain the proper stability of a supersaturated SLB solution and improve the oral bioavailability of the drug.

2. Materials and methods

2.1. Materials

Silybin was donated by Tianjin Tasly Pharmaceuticals Co., Ltd. (Tianjin, China). Soluplus and PVPVA were kindly donated by BASF (Ludwigshafen, Germany). Coumarin-6 was purchased from Sigma–Aldrich (Saint Louis, Missouri, USA). RPMI 1640 medium and 0.25% trypsin were obtained from Invitrogen (Ontario, CA, USA). Fetal bovine serum was purchased from Sijiqing Biological Engineering Materials Co., Ltd. (Zhejiang, China). Heparin sodium (>150 IU/mg) and isoflurane were obtained from the Sinopharm Chemical Reagent Co., Ltd. (Shanghai, China). Acetonitrile and methanol of HPLC grade were purchased from Tedia Company, Inc. (Fairfield, OH, USA). A Milli-Q water purification system was used to prepare water (Millipore Corp., Billerica, MA, USA). All other chemicals used were of analytical reagent grade and were purchased locally.

2.2. Methods

2.2.1. Supersaturation tests

Supersaturation was investigated using the solvent-shift method[24,25]. Briefly, 30 mg of SLB dissolved in dimethyl sulfoxide was added to 100 mL of Milli-Q water containing 1.2 mg/mL Soluplus/PVPVA at different ratios. Then, 2 mL samples were taken at various time points including 0.5, 1, 2, 3, and 4 h (without replacement) and filtered through a 0.45-μm filter. The filtrate was immediately diluted with an appropriate volume of the mobile phase to prevent precipitation and injected into the HPLC system for analysis.

The SLB concentration in the filtrate was analyzed using an Agilent 1200 high-performance liquid chromatography system (Agilent, USA), consisting of a G1311A quaternary pump, a G1315D diode array detector set at wavelength 288 nm, a G1329B high-performance autosampler and a G1316A thermostatted column compartment set at 40 °C. The system was operated under isocratic conditions with a flow rate of 1 mL/min using a mobile phase of acetonitrile/water (48/52, *v*/*v*) and an Agilent Eclipse XDB-C18 (250 mm × 4.6 mm, 5 μm) column.

To examine the degree of supersaturation as a function of time, we referred to a previously reported method[26] and plotted the curve of the drug concentration over time as the degree of a supersaturation-time curve. The supersaturation factor (SF) was calculated as Eq. (1):

$$SF = \frac{AUC_{0.5-4h}\ (\text{without polymer})}{AUC_{0.5-4h}\ (\text{a saturated solution})} \quad (1)$$

where $AUC_{0.5–4h}$ (without polymer) was the area under the curve of the non-polymer supersaturation-time profile; $AUC_{0.5–4h}$ (a saturated solution) was the area under the curve for a saturated solution. This calculation is illustrated in Fig. 1A, where the SF for SLB is given by Eq. (2):

$$SF = \frac{\text{Area A} + \text{Area B}}{\text{Area A}} \quad (2)$$

To assess the extent to which excipients stabilize supersaturation, the excipient gain factor (EGF) was calculated by Eq. (3):

$$\mathrm{EGF} = \frac{\mathrm{AUC}_{0.5-4\mathrm{h}}\ (\text{with polymer})}{\mathrm{AUC}_{0.5-4\mathrm{h}}\ (\text{without polymer})} \quad (3)$$

where $\mathrm{AUC}_{0.5-4\mathrm{h}}$ (with polymer) was the area under the curve of the supersaturation-time profile with polymer. Based on Fig. 1A, the excipient gain factor of polymers for SLB was calculated as Eq. (4):

$$\mathrm{EGF} = \frac{\text{Area A} + \text{Area B} + \text{Area C}}{\text{Area A} + \text{Area B}} \quad (4)$$

2.2.2. *Cellular uptake study using formulations loaded with the fluorescent probe coumarin-6*

For cellular uptake study, supersaturated solutions with PVPVA (SDDS-P), Soluplus (SDDS-S) and their mixtures (Soluplus: PVPVA = 2:8, *v/v*) (SDDS-SP) loaded with high and low concentrations of the fluorescent probe coumarin-6 were prepared. Briefly, polymers (360 mg) and coumarin-6 were dissolved in 4 mL of chloroform, and the solvent was evaporated under vacuum at 30 °C to form a homogeneous solid film. The resulting film was stored overnight in vacuum at 40 °C for drying. The final products were dispersed in 15 mL water at 37 °C with magnetic stirring at 400 rpm (IKA RET basic, IKA, China) for 1 h to obtain a supersaturated solution. The concentration of coumarin-6 in the sample solution was determined by microplate reader (Infinite™ 200, Tecan Group Ltd., Switzerland) by using excitation and emission wavelengths of 465 and 520 nm, respectively. The test samples were diluted 20-fold with Hank's balanced salt solution (HBSS) to obtain a final concentration of 500 ng/mL (HF) or 50 ng/mL (LF) for the cellular uptake study. Confocal laser scanning microcopy (CLSM) and flow cytometry analysis (FCM) were used to assess the intracellular uptake efficiency of these formulations.

Caco-2 cells were seeded on glass cover slips and directly added to 12-well plates at a density of 1×10^5 cells per well for CLSM and flow cytometry analysis. After culturing for 2 days, the culture medium was discarded, and the cells were incubated with 1 mL of the respective formulations for 2 h at 37 °C. For CLSM analysis, the cell nuclei were stained using 4′,6-diamidino-2-phenylindole (DAPI, 5 μg/mL, Beyotime, Shanghai, China), and the samples were visualized using a confocal inverted microscope FV1000 (Olympus, Tokyo, Japan). For flow cytometry analysis, the cells were trypsinized for 2 min with 0.25% trypsin, and the enzymatic activity was then stopped by the addition of culture medium. After centrifugation at 1000 rpm (Allegra 64R, Beckman, USA) for 3 min, the culture medium was discarded and the treated cells transferred to flow cytometry tubes. The cells were analyzed by a BD FACSCalibur fluorescent-activated flow cytometer with BD Cell Quest software (BD Bioscience, Le Pont-de-Claix, France). This experiment was performed in triplicate, and a total of 10,000 cells per sample were analyzed.

2.2.3. *Transport of SLB in supersaturated micelle complex across Caco-2 cell monolayers*

SLB-loaded supersaturated polymeric micelles consisting of PVPVA (SDDS-P), Soluplus (SDDS-S) and a mixture of PVPVA and Soluplus (Soluplus: PVPVA = 2:8, *v/v*) (SDDS-SP) were prepared by solvent evaporation methods. Briefly, 400 mg of SLB and 1600 mg of polymer were dissolved in 60 mL of a 5:1 mixture of acetone and ethanol. The majority of the solvent was then removed by evaporation using a rotary evaporator, while the remaining solvent was removed from the viscous liquid by placing it on a glass plate in vacuum at 40 °C overnight. Then, the product was scratched from the plate and ground using a mortar and pestle. Finally, samples equivalent to 30 mg of SLB were dispersed in 15 mL water and stirred at 500 rpm (IKA RET basic, IKA, China) for 2 h at

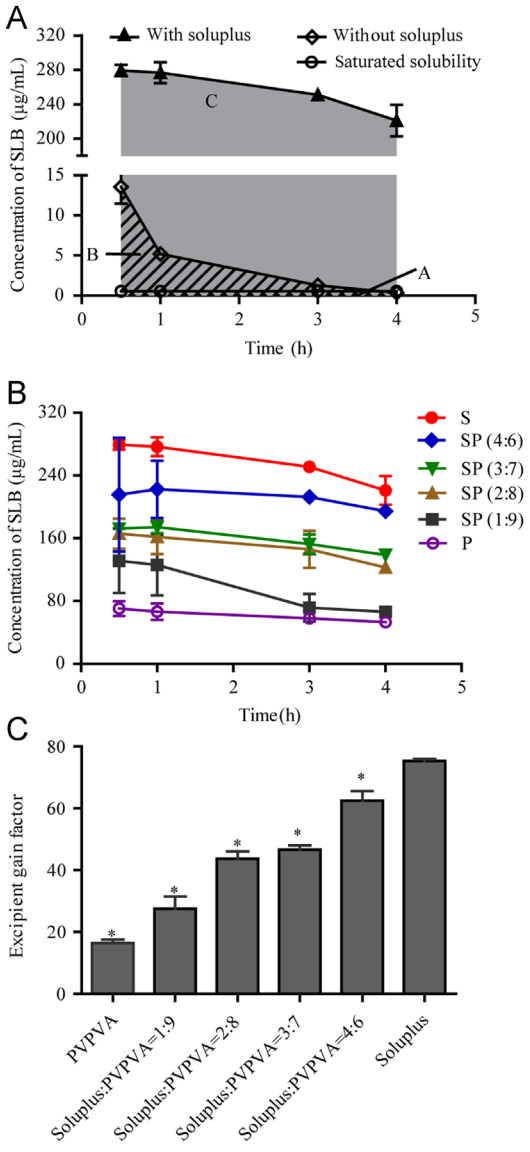

Figure 1 (A) Schematic illustration of the degree of supersaturation-time profile, exemplified by the Soluplus group. Area A: the area under the saturation profile of SLB in milli-Q water; Area B: the area under degree of supersaturation-time profiles of SLB in milli-Q water; Area C: milli-Q water with 1.2 mg/mL Soluplus (area C) upon solvent shift. Mean ± SD, (n = 3). (B) Effect of different ratios of Soluplus/PVPVA (SP) on the maintenance of SLB supersaturation. (C) Mean excipient gain factors of the different excipients for the supersaturated SLB solution. Values were expressed as the mean ± SD, n = 3. Bars indicated with * on top represent a significant difference *versus* Soluplus group.

37 °C. The mixture was filtered through a 0.45-μm mixed cellulose ester membrane to obtain a homogeneous polymeric micellar solution.

Cells were seeded onto Transwell polycarbonate cell culture inserts (12 mm diameter, 0.4 μm pore size, Costar, Corning Costar Co., Cambridge, MA, USA) at a density of 1×10^5 cells per well and incubated for 21–25 days to reach confluence. The integrity of the Caco-2 monolayer was evaluated both before and immediately after the transport studies using a Millicell-ERS (Millipore, Bedford, MA, USA). Monolayers with transepithelial electric resistance (TEER) values above 200 Ω/cm^2 were considered to have good integrity.

The cell monolayer was equilibrated with HBSS at 37 °C 30 min before the beginning of the experiment. Then, 0.5 mL of HBSS-diluted supersaturated SLB solution containing 100 μg/mL SLB was added to the AP (donor) compartments and 1 mL HBSS to the receiver chamber. At predetermined time points including 15, 30, 60, 90, 120, 180, and 240 min, 400 μL aliquots were withdrawn from the receiver chamber and replaced with an equivalent volume of HBSS to maintain a constant receiver fluid volume. The samples were centrifuged at 12,000 rpm (Allegra) for 10 min, and the supernatant was collected and injected into the HPLC system for analysis. All experiments were performed in triplicate. The apparent permeability coefficients (P_{app}) of SLB across Caco-2 monolayers were calculated according to the Eq. (5):

$$P_{app} = \frac{dQ/dt}{AC_0} \tag{5}$$

where C_0 (μg/mL) is the initial concentration of SLB in the donor, dQ/dt is the transport rate (μg/mL/s), and A is the surface area of the membrane filter (1.13 cm^2).

2.2.4. *Mechanism studies: interaction behavior between Soluplus and PVPVA*

2.2.4.1. Equilibrium solubility. To evaluate the effect of PVPVA on the solubilizing ability of Soluplus, the equilibrium solubility of SLB in distilled water containing various PVPVA concentrations with or without Soluplus were measured at 37 °C. The measurements were performed in triplicate using the shake flash method. Briefly, excess SLB was added to each PVPVA solution or mixed solution in a glass vial to form a suspension. The vial was sealed and kept in a biological shaker (SPH-100F, Shanghai, China) at 100 rpm for 24 h. The suspension was then centrifuged at 12,000 rpm (Allegra) for 15 min. The supernatant was carefully collected, and 20 μL was injected into the HPLC system for analysis.

2.2.4.2. Particle size determined by dynamic light scattering. A series of Soluplus-PVPVA mixed solutions with a Soluplus concentration of 1 mg/mL and PVPVA concentrations of 0, 1, 2, 4, 7, 10, and 20 mg/mL were prepared. Particle size was determined using a Zetasizer (Nano-ZS, Malvern instruments, UK) at 25 °C. Each sample was measured in triplicate.

2.2.4.3. Morphology observed by transmission electron microscopy. The morphology of the prepared PVPVA, Soluplus and Soluplus–PVPVA complex was observed using a transmission electron microscope (TEM). Polymer solutions with a concentration of 0.5 mg/mL were mixed with an equal volume of 2% phosphotungstic acid solution, and then a drop of the resulting solution was spread on a copper grid to form a coating and the excess liquid removed with filter paper. Samples were dried at room temperature for 10 min and viewed under a transmission electron microscope (Tecnai G2 Spirit 120 kV, FEI).

2.2.4.4. Aggregation behavior of Soluplus studied using pyrene fluorescence. The effect of PVPVA on the aggregation behavior of Soluplus was determined by the fluorescence probe pyrene. A stock solution of pyrene (6×10^{-4} mol/L) was prepared in acetone. Then, 100 μL of pyrene solution was placed into a volumetric flask and diluted to 6×10^{-7} mol/L pyrene, and the acetone was evaporated by vacuum drying. A specific volume of PVPVA was then added to the flask containing pyrene and diluted with water in separate microfuge tubes to obtain a series of solutions with concentrations of 0, 1, 2, 5, 10, 15, 20, 25, 30 and 40 μg/mL. A series of solutions with or without PVPVA (30 μg/mL) were obtained by similar methods. All those solutions were allowed to mix thoroughly for 24 h at 37 °C and then analyzed by a fluorescence spectrophotometer (F-4600, Hitachi, Japan). The emission spectrum of pyrene was obtained with an excitation wavelength of 334 nm. The emission wavelength was scanned from 350 to 500 nm with a scanning speed of 240 nm/s. The ratios of emission intensity at the peaks at 373 and 384 nm (I_{373}/I_{384}) were measured for solutions containing different polymer concentrations. The excitation and emission slits were 5.0 and 2.5 nm, respectively. The photomultiplier voltage was 600 V.

2.2.4.5. Thermodynamics study. The thermodynamics of the interaction between Soluplus and PVPVA were studied using isothermal titration calorimetry (ITC, MicroCal iTC200, Malvern instruments Ltd., UK). Soluplus and PVPVA powder were accurately weighed and dissolved separately in Milli-Q water. PVPVA solution in the titration syringe was added to Soluplus solution in the sample cell. The Milli-Q water was added as a reference for the heat balance of the sample cell. Another control experiment was performed to detect the effect of the PVPVA dilution heat. The thermodynamic parameters were then determined by nonlinear least-squares analysis of the binding isotherm using the independent binding site model in the Origin software (version 5.0) provided by MicroCal.

ITC directly estimates the binding thermodynamics by measurement of the energy of molecular interaction under specific conditions[27,28]. A series of data points in the thermograms represent the amount of heat released or absorbed per mole of injectant. The thermodynamic binding parameters are then determined by nonlinear least-squares analysis of the binding isotherm. The adjustable parameters in these fits are ΔH, the change in enthalpy (kcal/mol) upon binding; K_a, the association constant; and n, the number of binding sites per monomer of the molecule in the cell. From Eq. (6):

$$\Delta G = -RT\ln K_a \tag{6}$$

the reaction free energy ΔG (Kcal/mol) can be calculated. By the Gibbs free energy Eq. (7)

$$\Delta G = \Delta H - T\Delta S \tag{7}$$

the binding entropy at the experimental temperature can be calculated.

2.2.5. Pharmacokinetics study in rats

2.2.5.1. Animal experiments. Male Sprague–Dawley rats (body weight 300 ± 20 g) were obtained from the Medical Animal Test Center of Shanghai Institute of Materia Medica (Shanghai, China). The rats were randomly divided into 4 groups, each group containing 6 animals, and were orally administered with the different formulations (SLB-loaded SDDSs) at a dose of 200 mg/kg body weight. The rats were fasted for 12 h prior to the experiments, but allowed free access water. The food was only allowed to the rats 4 h after oral administration of formulations. Four hundred microliters of blood was collected *via* the orbital venous plexus under isoflurane anesthesia at various time points including 0.25, 0.5, 1, 1.5, 2, 3, 4, 6, 8, and 12 h post administration. The blood was centrifuged at 4000 rpm (Allegra) for 5 min, and separated plasma was collected in fresh tubes and stored at –20 °C till further use. All experiments were performed according to the Shanghai Institute of Materia Medica guidelines for experimental animal care.

2.2.5.2. Analysis of SLB in plasma. Twenty microliters of internal standard solution (α-naphthol, 5 μg/mL) and 200 μL of potassium dihydrogen phosphate (25 mmol/L) were added to a 150-μL plasma sample and vortexed for 1 min. Then, 4 mL of diethyl ether was added as an extraction solvent, and the mixture was vortexed again for 10 min. After centrifugation at 5000 rpm (Allegra) for 10 min, the organic phase was carefully transferred to a fresh microfuge tube. The remaining SLB was further extracted by adding 4 mL of diethyl ether. The collected organic phase was then evaporated to dryness at 40 °C under a gentle stream of nitrogen. The dried residue was redissolved in 100 μL of mobile phase, and 40 μL of the sample was injected into the HPLC system with an Agilent Eclipse XDB-C18 column (250 mm × 4.6 mm, 5 μm). The mobile phase consisted of methanol and pH 4.0 phosphoric acid solution (48:52, *v*/*v*) at a flow rate of 1 mL/min. The effluent was monitored at 288 nm.

2.2.5.3. Pharmacokinetic analysis. The main pharmacokinetic parameters of silybin, including the area under the plasma concentration–time curve (AUC), the maximal plasma concentration of silybin (C_{max}) and the time to reach C_{max} (T_{max}), were calculated using noncompartmental analysis by the DAS 2.0 software package (Mathematical Pharmacology Professional Committee of China, Shanghai, China).

2.3. Data analysis

One-way analysis of variance (ANOVA) was used for comparison among groups. Differences were considered statistically significant at $P < 0.05$.

3. Results and discussion

3.1. Excipient-mediated precipitation inhibition in supersaturated SLB solution

To examine the degree of supersaturation as a function of time, a supersaturated solution of SLB was prepared using the solvent-shift method, followed by determination of the free drug concentration. Once the dissolved SLB in DMSO was added into aqueous solution, the drug clearly precipitation because SLB was highly supersaturated in this solution. Based on the obtained solubility values (0.54 μg/mL), the "supersaturation factor", expressed as the ratio of the area under the degree of supersaturation-time profiles up to 4 h ($AUC_{0.5–4h}$) and the $AUC_{0.5–4h}$ for a saturated solution, was calculated to be 22.2 ± 1.19. However, the presence of polymer delayed the progress of crystallization (Fig. 1B). The antiprecipitation ability of PVPVA is relatively weak, and the supersaturation concentration of SLB in the PVPVA solution was approximately 50 μg/mL after 1 h. However, Soluplus inhibited precipitation relatively strongly and kept the concentration of SLB above 200 μg/mL in 4 h. When the antiprecipitation ability of the mixture of Soluplus and PVPVA was analyzed by taking a series of Soluplus and PVPVA ratios, it was observed that the anti-precipitation ability was significantly enhanced compared to that of PVPVA alone. This result suggested that Soluplus played an important role in precipitation inhibition.

To further assess the antiprecipitation ability of various polymers, we calculated the "excipient gain factors" to make more concise comparisons. As shown in Fig. 1C, as the ratio of Soluplus increased, the anti-precipitation ability significantly improved ($P < 0.05$).

3.2. The cellular uptake mechanism of drug in Soluplus-PVPVA complex

The cellular uptake of Soluplus-PVPVA was observed and quantified *via* CLSM and FCM using the hydrophobic probe coumarin-6. As shown in Fig. 2A and B, for the LFs, no significant difference could be detected among SDDS-S, SDDS-P and SDDS-SP, while for the HFs, the cellular uptake of coumarin-6 in SDDS-SP was significantly higher than that in SDDS-S and SDDS-P. The fluorescence intensity of cells incubated with SDDS-SP was approximately two-fold higher than that of cells incubated with SDDS-P and SDDS-S, which showed similar fluorescence intensity. It has been addressed that the presence of solubilizing additives can decrease cellular uptake[18] due to the effect of the solubility-permeability trade-off[19], and only the unionized free drug is considered to be able to undergo passive absorption. Previously, we have proved that increasing the usage of Soluplus resulted in a diminishing uptake amount of the drugs because the drugs were released with difficulty[16]. Therefore, we could reasonably assume that the drugs incorporated in our SDDS were released before the transcellular process. For the three LFs, the coumarin-6 molecules were almost completely solubilized, and no supersaturated solutions formed; thus, there were no significant cellular uptake differences among them. For the HFs, supersaturated solutions of coumarin-6 were introduced (coumarin-6 precipitation could be seen after 48 h of encapsulation). In the case of SDDS-S, the coumarin-6 molecules were almost entirely solubilized by Soluplus micelles, resulting in decreased cellular uptake[16]. However, in the case of SDDS-P, the coumarin-6 was highly supersaturated and precipitated rapidly after hydration, also resulting in low uptake. In the case of SDDS-SP, it was observed that supersaturated solutions of coumarin-6 could form a sustained delivery system (coumarin-6 precipitation could be observed only after 24 h of encapsulation), which could help to further improve the cellular uptake[29]. Although Soluplus had the best antiprecipitation ability, the Soluplus-PVPVA complex had higher cellular uptake. These observations confirmed that SDDS exhibiting higher and proper stable supersaturation is more conducive to drug uptake.

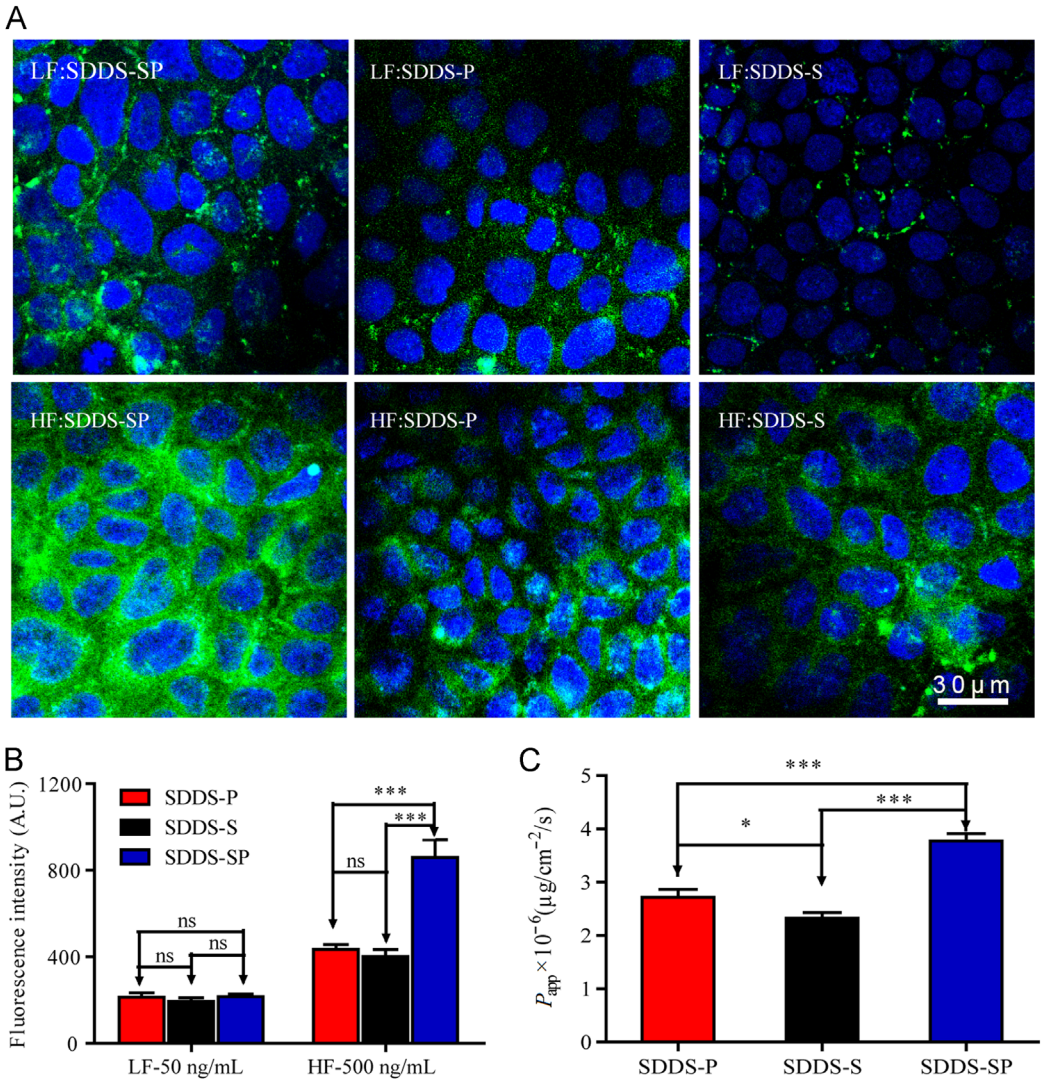

Figure 2 (A) Laser scanning confocal microscope images of Caco-2 cells after 2 h of incubation with coumarin-6 loaded SDDS-S, SDDS-P and SDDS-SP. (B) Quantitation of fluorescence intensity of coumarin-6 uptake by cells, determined by flow cytometry. (C) P_{app} of SLB in AP to BL direction for SDDS-S, SDDS-P and SDDS-SP (2:8, *v/v*) formulations. Error bars represent standard deviation, $n=3$. $^{*}P<0.05$ and $^{***}P<0.001$ for the indicated comparison, and ns indicates no statistical difference. Scale bar: 30 μmol/L.

3.3. Effects of Soluplus–PVPVA complex on transport of SLB across Caco-2 monolayers

To evaluate the effect of the Soluplus–PVPVA complex on SLB transport through cell monolayers, the apparent permeability coefficient (P_{app}, μg/cm^2/s) of SLB from the AP to the BL side was determined, and the results are shown in Fig. 2C. The P_{app} of SDDS-SP was significantly higher than those of SDDS-P and SDDS-S. The overall order of the P_{app} of these formulations was found to be as follows: SDDS-SP > SDDS-P > SDDS-S. Although Soluplus could maintain a high degree of supersaturation, we considered it more crucial to achieve a high free drug concentration. We demonstrated that SDDS-SP could greatly concentrate the drug at the absorption site and enhance transcellular transport in the free form.

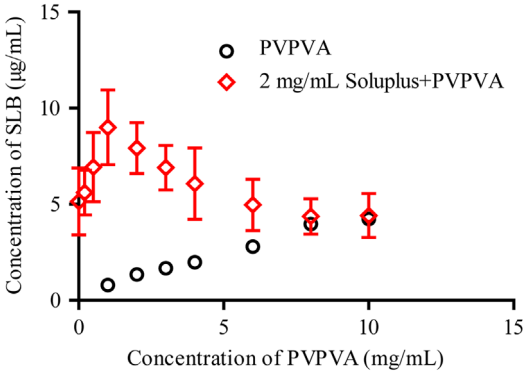

Figure 3 Effect of PVPVA on the solubilization ability of Soluplus. Values are expressed as the mean ± SD, $n=3$.

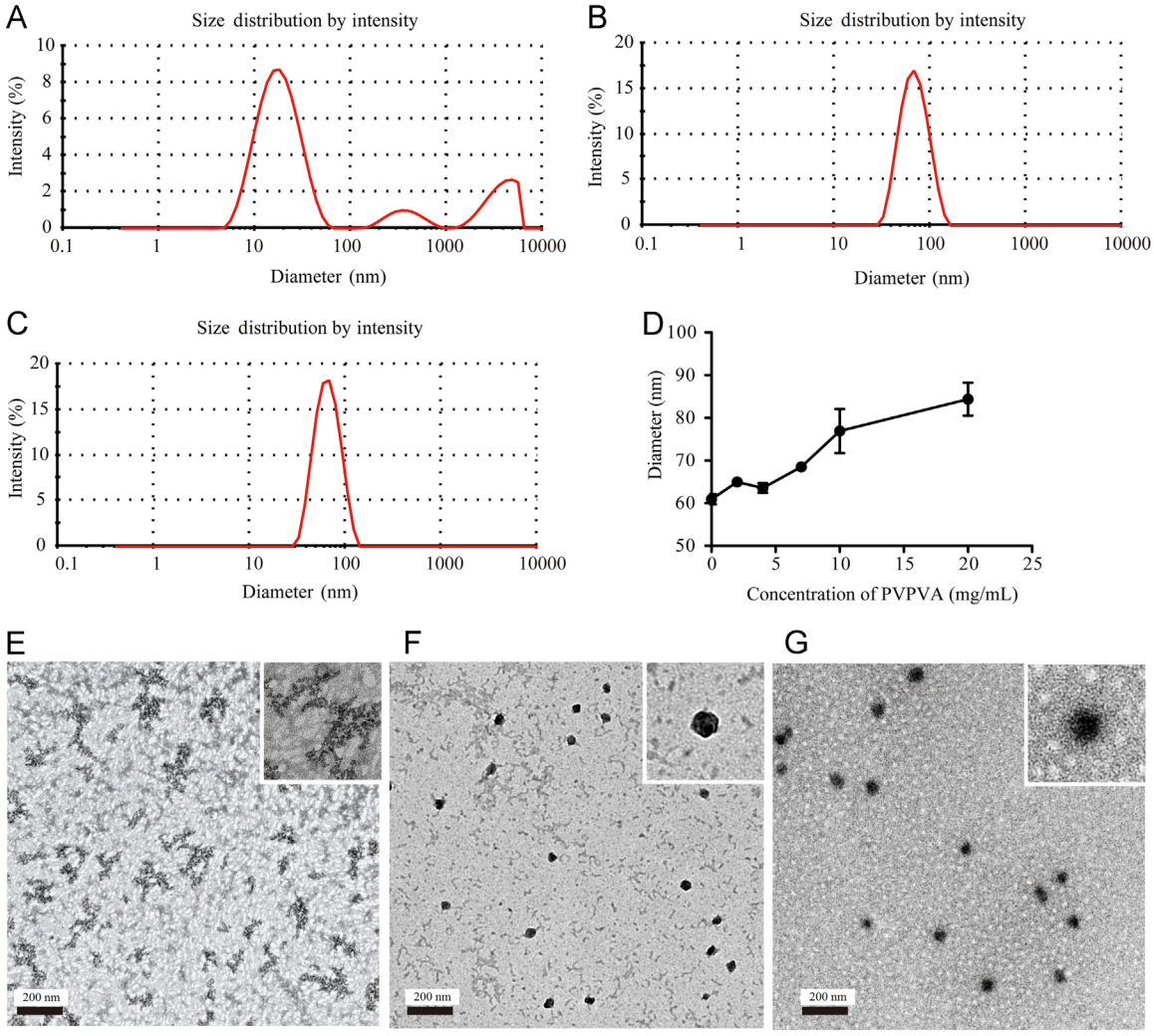

Figure 4 Size distributions of (A) PVPVA; (B) Soluplus; and (C) Soluplus-PVPVA (2:8, *v/v*) complex measured by dynamic light scattering. (D) Effect of the concentration of PVPVA on the size of Soluplus micelles. Values are expressed as the mean ± SD, $n = 3$. TEM photographs of (E) PVPVA, (F) Soluplus and (G) Soluplus/PVPVA (2:8, *v/v*) complex (scale bar: 200 nm).

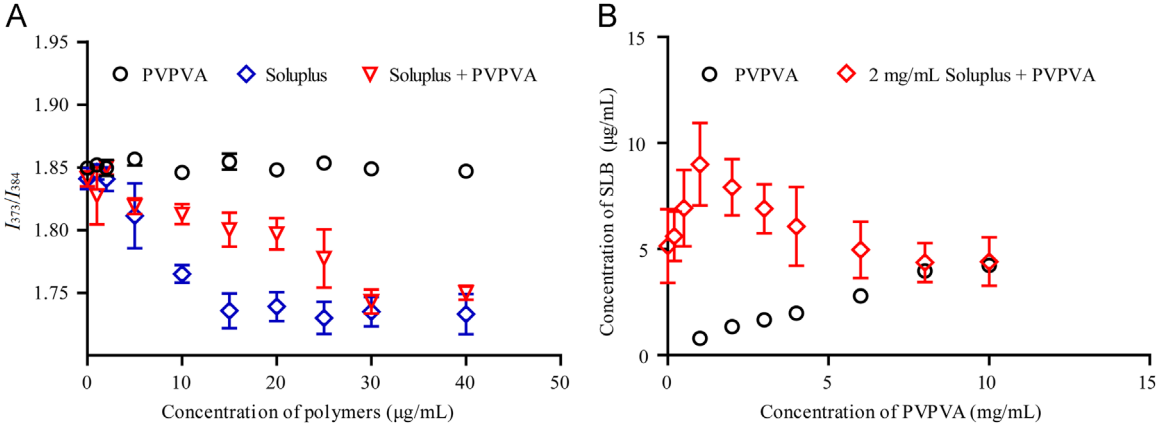

Figure 5 (A) The spectrum of pyrene luminescence. (B) The fluorescence intensity ratio I_{373}/I_{384} of pyrene in solutions with different concentrations of PVPVA, Soluplus, and Soluplus+30 μg/mL PVPVA. Values are expressed as the mean ± SD, $n = 3$.

3.4. *Mechanism by which the Soluplus-PVPVA complex promotes the oral absorption of hydrophobic drugs*

3.4.1. *Effect of PVPVA on the solubilization ability of Soluplus*

We studied the effect of PVPVA on the solubilization ability of Soluplus by measuring the equilibrium solubility of SLB (Fig. 3). The solubility of SLB in water is very low (0.5 μg/mL). However, this solubility can be effectively increased in the presence of Soluplus and was raised to 5 mg/mL when a Soluplus concentration of 2 mg/mL was used. PVPVA also has a weaker solubilizing effect on SLB, and a linear correlation was observed with increasing polymer concentration. For the Soluplus–PVPVA mixed solution, it was observed that when PVPVA was added to the Soluplus solutions, the solubilizing ability of Soluplus for SLB improved significantly. However, further increasing the amount of PVPVA in to Soluplus solution resulted in a decrease of solubilizing ability of Soluplus to SLB. Since the solubilization effect of polymers is related to the hydrophobic core of the micelle, we speculate that the addition of PVPVA to the Soluplus solution led to a structural change in the Soluplus micelles.

3.4.2. *Particle size of Soluplus-PVPVA complex*

Due to the amphipathic polymeric nature of Soluplus, it can spontaneously form micelles approximately 60 nm in diameter in aqueous solution. We investigated the effect of PVPVA on the micelle size of Soluplus by dynamic light scattering (Fig. 4). The dynamic light scattering results of PVPVA samples was exhibiting multiple peaks with a polydispersity index (PDI) 0.7, suggesting that the size of PVPVA complexes in aqueous solution was not uniform (Fig. 4A). A uniform size distribution of Soluplus micelles was formed with a diameter of 60 ± 0.71 nm and PDI 0.072 ± 0.026 (Fig. 4B). However, with the addition of PVPVA to the Soluplus, the micelle size was between 60 and 80 nm with PDI < 0.2 (Fig. 4C and D). Thus, we speculated that PVPVA and Soluplus may form a homogeneous complex with a slightly increase in the micelle size compared to that of micelles formed from Soluplus alone.

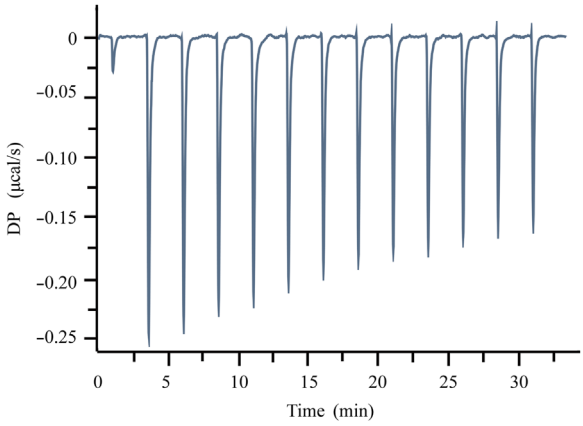

Figure 6 Isothermal titration calorimetry (ITC) profiles of PVPVA with Soluplus.

To obtain direct evidence of the mixed micelles, we carried out TEM to characterize PVPVA, Soluplus, and the Soluplus/PVPVA (2/8) complex. As shown in Fig. 4E, the morphology of PVPVA was found to be irregular in shape, while the micelles of Soluplus (Fig. 4F) and Soluplus/PVPVA (Fig. 4G) were found to be uniform and nearly spherical in shape. The results of TEM confirmed the existence of the Soluplus/PVPVA complex.

3.4.3. *Aggregation behavior of Soluplus studied using pyrene fluorescence*

Pyrene, a hydrophobic fluorescent probe, has five electron emission peaks in its fluorescence emission spectra (Fig. 5A) in aqueous solution, at 373, 379, 384, 394 and 480 nm. The ratio of fluorescence intensity at 373 nm and 383 nm (I_{373}/I_{384}) depends largely on the polarity environment of the pyrene molecule[30,31]. Therefore, the difference in the micropolarity of Soluplus micelles and the Soluplus–PVPVA complex could be predicted by fluorescence spectroscopy, according to comparison of their vibrational structures, as the pyrene ratio of the first band to the third band (I_{373}/I_{384}) is a measure of polarity.

The fluorescence intensity ratio I_{373}/I_{384} of pyrene solutions with different concentrations of PVPVA, Soluplus, and Soluplus + 30 μg/mL PVPVA are shown in Fig. 5B. Analysis of the fluorescence intensity of PVPVA solution at 373 nm and 383 nm did not reveal any change in the fluorescence ratio when the concentration of PVPVA was less than 40 μg/mL, indicating that the PVPVA solution did not form micelles. In contrast, a sharp change in the I_{373}/I_{384} intensity occurred in the range of 2–10 μg/mL Soluplus, indicating that the critical micelle concentration of Soluplus is within this range. In the presence of 30 μg/mL of PVPVA, the I_{373}/I_{384} fluorescence ratio decreased slowly with increasing Soluplus concentration between 2 and 15 μg/mL, exhibited a sharp decline between 20 and 30 μg/mL Soluplus and then remained stable. This result suggested that PVPVA interacts with Soluplus to form a complex and that two conformational changes of Soluplus occur.

3.4.4. *Thermodynamics study of the interaction between Soluplus and PVPVA*

The thermal titration profile of the reaction between PVPVA and Soluplus is shown in Fig. 6, and the parameters are presented in Table 1. The reaction binding heat results from the combined enthalpy and binding entropy. The enthalpy reflects the strength of interaction due to the formation of hydrogen bonds and van der Waals interactions. The entropy reflects the hydrophobic interactions between PVPVA and Soluplus and the conformational change that occurs in the formation of the complex. In this case, the reaction between PVPVA and Soluplus is a weak exothermic reaction, and ΔG (free energy), ΔH, and $-T\Delta S$ are all negative with values of –6.37, –3.4 and –2.97, respectively, indicating that the reaction is carried out in the Soluplus–PVPVA complex and is driven by both entropy and enthalpy.

Table 1 Thermodynamic parameters of PVPVA with Soluplus at 25 °C.

K_a (10^{-6})	ΔG (kcal/mol)	ΔH (kcal/mol)	$-T\Delta S$ (kcal/mol)	n (sites)
21.5	–6.37	–3.4	–2.93	3.49

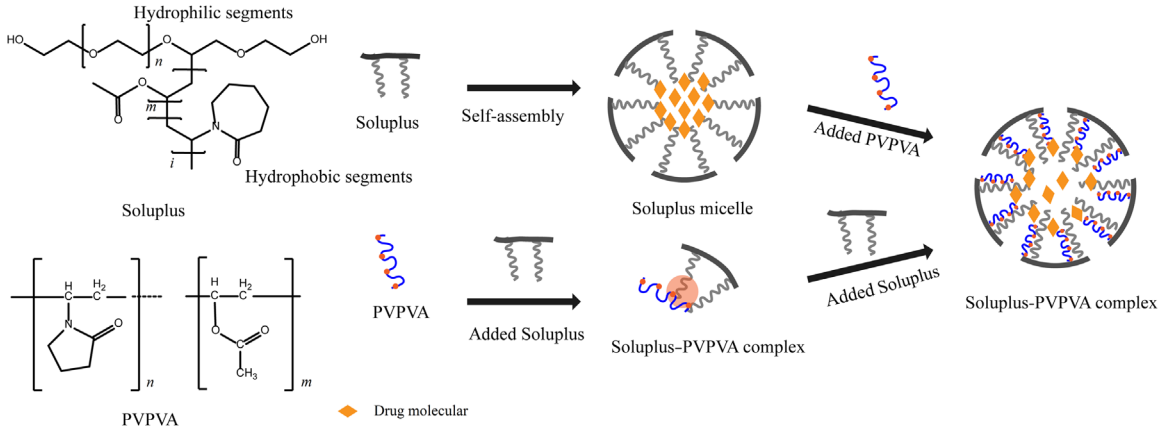

Figure 7 Illustration of Soluplus–PVPVA complex in water.

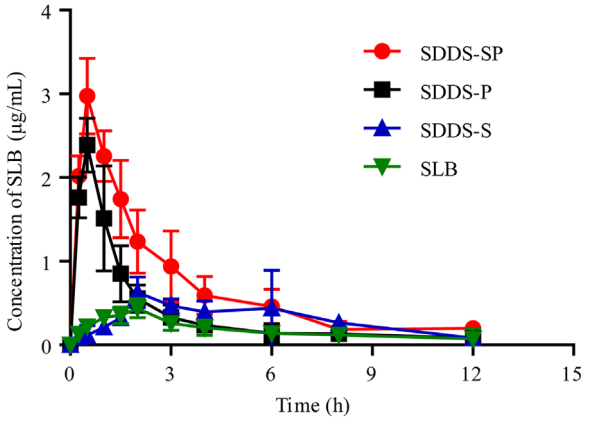

Figure 8 Mean SLB concentration in blood *versus* time profiles following the oral administration of SLB-loaded SDDSs and SLB powder. Error bars represent standard deviation, $n=6$.

Table 2 Pharmacokinetic parameters after the oral delivery of SLB-loaded SDDSs.

Parameter	C_{max} (μg/mL)	T_{max} (h)	$AUC_{0-\infty}$ (μg · h/mL)
SDDS-P	$2.4\pm0.3^{**}$	0.5 ± 0.0	$5.8\pm1.5^{***,\#\#\#}$
SDDS-S	$0.8\pm0.2^{**}$	3.3 ± 2.3	$4.2\pm1.4^{**,\#\#\#}$
SDDS-SP	$3.0\pm0.5^{**}$	0.5 ± 0.0	$9.5\pm0.8^{***}$
SLB	0.4 ± 0.1	2.0 ± 0.0	2.1 ± 0.4

$AUC_{0-\infty}$, the area under the blood drug concentration–time curve; C_{max}, the maximal blood concentration of the drug; T_{max}, the time taken to reach C_{max}. Values are expressed as the mean ± SD ($n=6$).
$^{**}P<0.01$;
$^{***}P<0.001$ *versus* SLB group;
$^{\#\#\#}p<0.001$ *versus* SDDS-SP group.

3.4.5. *Mechanism by which the Soluplus-PVPVA complex promotes the oral absorption of hydrophobic drugs*

According to the results reported above, we have summarized the possible formation mechanisms of the Soluplus-PVPVA complex in Fig. 7. Due to the presence of both hydrophilic and hydrophobic residues, Soluplus self-aggregates to form micelles, with SLB encapsulated in the hydrophobic core. The amount of SLB transported across the Caco-2 monolayer in SDDS-S was limited due to its strong interactions with the hydrophobic core of the Soluplus micelles. When PVPVA was added to the Soluplus micelle solutions, hydrophobic interactions between PVPVA and Soluplus could occur, which hindered the hydrophobic interaction between SLB and the Soluplus micelle cores. We have recently demonstrated that amphiphilic sodium dodecyl sulfate (SDS) molecules can enter the Soluplus micelle cores and lead to the breakage of the Soluplus micelle structure[32]. However, the PVPVA was unable to destabilize the Soluplus micelles by entering the micellar structure due to its large size and hydrophilic nature. Thus, there was a very high possibility for the hydrophilic region of the PVPVA polymer to bind to the polyethylene glycol chains of the Soluplus micelles, leading to their destabilization. The ITC results indicated that the interactions between PVPVA and Soluplus were driven by both entropy and enthalpy. Since the enthalpy reflects the formation of hydrogen bonds and van der Waals interactions, and the entropy reflects the hydrophobic interactions, we speculated that the PVPVA combined with the hydrophilic-hydrophobic boundary of the Soluplus micelles (Fig. 7). The pyrene fluorescence results bore out our supposition. When Soluplus was added to the PVPVA solution at concentrations from 2 to 15 μg/mL, the I_{373}/I_{384} fluorescence ratio decreased slowly, but a sharp decline was observed from 20 to 30 μg/mL. The change in the fluorescence ratio suggested that two conformational changes occurred in the reaction between Soluplus and PVPVA. When the concentration of Soluplus was below the critical micelle concentration (CMC), Soluplus was prone to aggregate with the hydrophobic groups of PVPVA to form a hydrophobic region. When the concentration of Soluplus exceeded the CMC, the hydrophobic chains of Soluplus aggregated itself to form a more hydrophobic region, resulting in micelle formation, and the PVPVA, which combined with Soluplus *via* hydrophobic interaction, then aggregated at the hydrophilic-hydrophobic boundary of the micelles. The new micelles had a smaller hydrophobic region of Soluplus molecules available to bind SLB. Therefore, we envisioned that the interaction between SLB and the micelles decreased. The observed decrease in the overall entrapment of SLB in the micelles and the increase in the cell transport of SLB validated our hypothesis.

3.5. *Pharmacokinetic study*

The plasma SLB concentration-time profiles following oral administration of three supersaturated formulations and SLB powder in Sprague–

Dawley male rats are presented in Fig. 8. The pharmacokinetic parameters including T_{max}, C_{max}, and $AUC_{0-\infty}$ are shown in Table 2.

The plasma profiles of various formulations of SLB were compared. The $AUC_{0-\infty}$ values from the administration of SDDS-P, SDDS-S and SDDS-SP were 5.8, 4.2, 9.5 μg h/mL, respectively, which were significantly higher than that of SLB powder (2.1 μg · h/mL, $P < 0.01$). This result suggests that SDDS effectively improved the oral bioavailability of SLB. At the initial time, the concentration of SLB in plasma for the SDDS-P formulation was very high, due to the weak precipitation inhibition ability of PVPVA, while the supersaturated solution of SLB produced by the solid dispersion in the gastrointestinal fluid would rapidly precipitate and crystallize, thus it can't be further absorbed. SDDS-S failed to achieve a high C_{max} but maintained a lower plasma concentration after 2 h administration, resulting in a much higher AUC than the SLB group ($P < 0.01$). For the SDDS-SP formulation, the C_{max} was found to be 3.0 μg/mL and was reached quickly in circulation. On the contrary, the Soluplus–PVPVA complex released in sustained fashion, resulted in a slow rate of clearance and a significantly higher AUC. The $AUC_{0-\infty}$ of SDDS-SP was found to be 4.5, 2.3 and 1.6-fold higher than SLB powder, SDDS-S and SDDS-P, respectively. These data provided strong evidence that the SDDS-SP complex improved the oral bioavailability of SLB and that the mixed carrier enhanced the absorption of SLB better than PVPVA or Soluplus alone. The Soluplus–PVPVA complex belonged to a supersaturated drug delivery system, and the supersaturation could increase the concentration of SLB in the GI tract for oral absorption. In addition, the decreased interaction between Soluplus and SLB caused by PVPVA could enhance the release of SLB from the Soluplus micelle core, which further increased the concentration of free drug in the GI tract for transmembrane translocation. Thus, the oral bioavailability of SLB was increased.

4. Conclusions

The main mechanism by which SDDSs promote the absorption of the loaded therapeutics is the increased passive transport of the free drugs. Therefore, improving the concentration of free drug in the gastrointestinal tract is the key to facilitate the oral delivery of poorly water-soluble drugs. Although Soluplus has a strong antiprecipitation effect, the release of the encapsulated drug in the gastrointestinal tract is very limited. PVPVA consists of long polymer chains that also contain both hydrophilic and hydrophobic groups. Our results suggest that hydrophobic region of PVPVA would interfere with the formation of the hydrophobic core of Soluplus, thus significantly decreasing the interaction between hydrophobic drugs such as SLB and the Soluplus core. Therefore, the solubilized SLB in the Soluplus–PVPVA complex decreased significantly compared to that in Soluplus micelles, which was further supported by the evidence of biophysical and spectroscopy studies. Furthermore, cellular uptake studies were performed using SDDS-S, SDDS-P and SDDS-SP formulations and showed higher cellular uptake of SDDS-SP formulations compared to SDDS-S and SDDS-P. The oral bioavailability of SLB in the SDDS-SP formulation was found to be significantly improved in a rat model. Thus, maintaining the proper stability of a supersaturated solution is very important for the SDDS. We expect this approach to be useful to the scientific community in enhancing the oral bioavailability of poorly water-soluble drugs.

Acknowledgments

This work was supported by the National Natural Science Foundation of China (grant Nos. 81573378 and 81773651) and the Shanghai Science and Technology Innovation Action Plan for Basic Research, China (No. 17430741500).

References

1. Brouwers J, Brewster ME, Augustijns P. Supersaturating drug delivery systems: the answer to solubility-limited oral bioavailability?. *J Pharm Sci* 2009;**98**:2549–72.
2. Lee DH, Yeom DW, Song YS, Cho HR, Choi YS, Kang MJ, et al. Improved oral absorption of dutasteride *via* Soluplus®-based supersaturable self-emulsifying drug delivery system (S-SEDDS). *Int J Pharm* 2015;**478**:341–7.
3. Ke Z, Zhang Z, Wu H, Jia X, Wang Y. Optimization and evaluation of oridonin-loaded Soluplus®–Pluronic P105 mixed micelles for oral administration. *Int J Pharm* 2017;**518**:193–202.
4. Yang M, Gong W, Wang Y, Shan L, Li Y, Gao C. Bioavailability improvement strategies for poorly water-soluble drugs based on the supersaturation mechanism: an update. *J Pharm Pharm Sci* 2016;**19**:208–25.
5. Taylor LS, Zhang GGZ. Physical chemistry of supersaturated solutions and implications for oral absorption. *Adv Drug Deliv Rev* 2016;**101**:122–42.
6. Gebauer D, Kellermeier M, Gale JD, Bergstrom L, Colfen H. Pre-nucleation clusters as solute precursors in crystallisation. *Chem Soc Rev* 2014;**43**:2348–71.
7. Warren DB, Benameur H, Porter CJ, Pouton CW. Using polymeric precipitation inhibitors to improve the absorption of poorly water-soluble drugs: a mechanistic basis for utility. *J Drug Target* 2010;**18**:704–31.
8. Zhang Y, Liu Y, Luo Y, Yao Q, Zhong Y, Tian B, et al. Extruded Soluplus/SIM as an oral delivery system: characterization, interactions, *in vitro* and *in vivo* evaluations. *Drug Deliv* 2016;**23**:1902.
9. Ogawa N, Hiramatsu T, Suzuki R, Okamoto R, Shibagaki K, Fujita K, et al. Improvement in the water solubility of drugs with a solid dispersion system by spray drying and hot-melt extrusion with using the amphiphilic polyvinyl caprolactam-polyvinyl acetate-polyethylene glycol graft copolymer and D-mannitol. *Eur J Pharm Sci* 2018;**111**:205–14.
10. Shi N, Zhang Y, Li Y, Lai H, Xiao X, Feng B, et al. Self-micellizing solid dispersions enhance the properties and therapeutic potential of fenofibrate: advantages, profiles and mechanisms. *Int J Pharm* 2017;**528**:563–77.
11. Shekhawat Prachi B, Pokharkar Varsha B. Understanding peroral absorption: regulatory aspects and contemporary approaches to tackling solubility and permeability hurdles. *Acta Pharm Sin B* 2017;**7**:260–80.
12. Shekhawat Prachi B, Pokharkar Varsha B. Understanding peroral absorption: regulatory aspects and contemporary approaches to tackling solubility and permeability hurdles. *Acta Pharm Sin B* 2017;**7**:260–80.
13. Quan G, Niu B, Singh V, Zhou Y, Wu C, Pan X, et al. Supersaturable solid self-microemulsifying drug delivery system: precipitation inhibition and bioavailability enhancement. *Int J Nanomed* 2017;**12**:8801–11.
14. Lee DR, Ho MJ, Jung HJ, Cho HR, Park JS, Yoon SH, et al. Enhanced dissolution and oral absorption of tacrolimus by supersaturable self-emulsifying drug delivery system. *Int J Nanomed* 2016;**11**:1109–17.
15. Song WH, Yeom DW, Lee DH, Lee KM, Yoo HJ, Chae BR, et al. *In situ* intestinal permeability and *in vivo* oral bioavailability of celecoxib in supersaturating self-emulsifying drug delivery system. *Arch Pharm Res* 2014;**37**:626–35.
16. Yu H, Xia D, Zhu Q, Zhu C, Chen D, Gan Y. Supersaturated polymeric micelles for oral cyclosporine A delivery. *Eur J Pharm Biopharm* 2013;**85**:1325–36.
17. Dahan A, Beig A, Lindley D, Miller JM. The solubility-permeability interplay and oral drug formulation design: two heads are better than one. *Adv Drug Deliv Rev* 2016;**101**:99–107.

18. Raina SA, Zhang GGZ, Alonzo DE, Wu J, Zhu D, Catron ND, et al. Impact of solubilizing additives on supersaturation and membrane transport of drugs. *Pharm Res* 2015;**32**:3350–64.
19. Dahan A, Miller JM. The solubility–permeability interplay and its implications in formulation design and development for poorly soluble drugs. *AAPS J* 2012;**14**:244–51.
20. Raina SA, Zhang G, Alonzo DE, Wu J, Zhu D, Catron ND, et al. Enhancements and limits in drug membrane transport using supersaturated solutions of poorly water soluble drugs. *J Pharm Sci* 2014;**103**:2736–48.
21. Mandal A, Bisht R, Rupenthal ID, Mitra AK. Polymeric micelles for ocular drug delivery: from structural frameworks to recent preclinical studies. *J Control Release* 2017;**248**:96–116.
22. Kamaly N, Yameen B, Wu J, Farokhzad OC. Degradable controlled-release polymers and polymeric nanoparticles: mechanisms of controlling drug release. *Chem Rev* 2016;**116**:2602–63.
23. Liu C, Chen Z, Chen Y, Lu J, Li Y, Wang S, et al. Improving oral bioavailability of sorafenib by optimizing the "Spring" and "Parachute" based on molecular interaction mechanisms. *Mol Pharm* 2016;**13**:599–608.
24. Yamashita T, Ozaki S, Kushida I. Solvent shift method for anti-precipitant screening of poorly soluble drugs using biorelevant medium and dimethyl sulfoxide. *Int J Pharm* 2011;**419**:170–4.
25. Alhalaweh A, Bergström CAS, Taylor LS. Compromised *in vitro* dissolution and membrane transport of multidrug amorphous formulations. *J Control Release* 2016;**229**:172–82.
26. Bevernage J, Brouwers J, Annaert P, Augustijns P. Drug precipitation–permeation interplay: supersaturation in an absorptive environment. *Eur J Pharm Biopharm* 2012;**82**:424–8.
27. Dam TK, Brewer CF. Thermodynamic studies of lectin–carbohydrate interactions by isothermal titration calorimetry. *Chem Rev* 2002;**102**:387–430.
28. Renaud JP, Chung CW, Danielson UH, Egner U, Hennig M, Hubbard RE, et al. Biophysics in drug discovery: impact, challenges and opportunities. *Nat Rev Drug Discov* 2016;**15**:679–98.
29. Miller JM, Beig A, Carr RA, Spence JK, Dahan A. A win–win solution in oral delivery of lipophilic drugs: supersaturation via amorphous solid dispersions increases apparent solubility without sacrifice of intestinal membrane permeability. *Mol Pharm* 2012;**9**:2009–16.
30. Zhao CL, Winnik MA, Riess G, Croucher MD. Fluorescence probe techniques used to study micelle formation in water-soluble block copolymers. *Langmuir* 1990;**6**:514–6.
31. Indulkar AS, Mo H, Gao Y, Raina SA, Zhang GGZ, Taylor LS. Impact of micellar surfactant on supersaturation and insight into solubilization mechanisms in supersaturated solutions of atazanavir. *Pharm Res* 2017;**34**:1276–95.
32. Xia D, Yu H, Tao J, Zeng J, Zhu Q, Zhu C, et al. Supersaturated polymeric micelles for oral cyclosporine A delivery: the role of Soluplus–sodium dodecyl sulfate complex. *Colloids Surf B Biointerfaces* 2016;**141**:301–10.